mmWaves RSSI Indoor Network Localization

Marco Vari
Department of Enterprise Engineering
University of Rome "Tor Vergata",
Rome, Italy
Email: marco.vari@uniroma2.it

Dajana Cassioli
Department of Information Engineering,
Computer Science and Mathematics,
University of L'Aquila, L'Aquila, Italy.
E-mail: dajana.cassioli@univaq.it

***Abstract*—Indoor positioning gained great interest in recent years. Several performance evaluations are available for consolidated systems, especially for ultra-wideband radios. Given the current success of mmWaves networks, in this paper, we investigate the performance of RSSI localization systems operating at mmWaves. Our reference is the IEEE 802.11ad standard for multi-Gbps WLANs. We tested the performance of RSSI localization in several scenarios differing in the number of access points serving as anchors and the RSSI acquisition. Our results show that RSSI localization is still effective at mmWaves using devices compliant with the IEEE 802.11ad standard in terms of sensitivity and frequency bands. We will show that these radios can achieve an accuracy of around 1 m if a sufficient number of measurement samples is acquired.**

I. Introduction

mmWaves radios are expected to provide very high data rate coverage for mobile, cellular and indoor applications [1], [2]. The great interest for mmWaves raised because of the huge available bandwidth for the unlicensed use in most countries around the world. The importance of localization at 60 GHz stems from applications that provide high data rate communications to individual users. The data rate can then be adjusted according to application and location. Thus, requirements on speed, capacity and security drive the need for mmWave solutions.

Promising received signal strength indicator (RSSI) localization systems have been studied extensively, but mainly at the WiFi, WiMax and ultra-wideband (UWB) bands [3]–[6]. Few publications are available on 60 GHz localization systems, mainly focusing on delay spread measurements at 60 GHz useful for systems utilizing Time-of- Arrival (TOA), Time-Difference-of-Arrival (TDOA) and Angle-of-Arrival (AOA) methods [7], [8].

The advantage of using 60 GHz lies in the high temporal resolution that can be achieved thanks to the very large available bandwidth (up to 7 GHz), which enables accurate range measurements. Furthermore, 60 GHz radio technology is the key player for indoor networking for fifth generation (5G) mobile wireless communications and is expected to embrace the modern approach of "small cell" deployment [9]. The short-range nature of 60 GHz signals, due to the high atmosferic absorption and the high path loss, makes these radios particularly suitable to implement this approach, thanks to the reduction of self-interference. The deployment of a capillary network of Access Points (APs) in the buildings can provide a simplification and an improvement of the localization task, thanks to the reduction of the coverage range of each AP.

In this paper we present a performance evaluation of RSSI localization in 60 GHz indoor networks operating in realistic conditions. Actually, our analysis is based on extensive simulations based on the path loss model of the 60 GHz channel derived in [10] from a large set of experimental data. We analyze the improvement that can be obtained by increasing the number of APs in the area, by using weighted combination of RSSI measurements, and by increasing the number of collected RSSI samples. Our model is based on the IEEE 802.11ad standard [11], hence it takes into account the typical (recommended) EIRP and receiver sensitivity. Although the considered RSS-based localization method is very simple, these systems are shown to achieve an accuracy of around 1 m, if specific requirements are fulfilled.

The paper is organized as follows. In Sec. II we describe the system model, with particular emphasis on the assumed path loss model based on actual 60 GHz channel measurements. In Sec. III we define the adopted algorithms to perform the trilateration RSS localization, and the strategies to improve the accuracy. The simulation parameters and the description of the simulation environment are provided in Sec. IV, whereas the results of our performance evaluation are shown and discussed in Sec. V. Finally, conclusions are drawn in Sec. VI.

II. System Model

We assume an area of 16×8.9 meters where a variable number of APs are appropriately located in order to guarantee maximum coverage. The APs are compliant with the IEEE 802.11ad standard [11], thus their EIRP is set to 10 dBm, and the three levels of receiver sensitivity specified by the standard are considered, namely -48 dBm, -63 dBm and -78 dBm. Each AP is assigned a frequency channel out of the four available channels defined by standard recommendations and frequency allocations at 60 GHz.

The signal strength at the receiver is calculated according to the path loss model for 60 GHz channels proposed in [10], which accounts for both distance and frequency dependence, as described in the following. Although the path loss model applies to different antennas' configurations, we assume that our system uses of omni-directional antennas at both the APs and terminals. All APs and terminals are assumed to be in line-of-sight (LoS).

978-1-4799-4640-2/14/$31.00 ©2014 IEEE

TABLE I
MEASUREMENTS' SETUP

MEASUREMENT	ANTENNAS (Gain - dB) Tx	Rx	DISTANCE (m)
LOS O-O	omni (2)	omni (2)	1 - 10 (Δ = 0.5)
LOS H_{15}-H_{15}	horn (15)	horn (15)	1 - 20 (Δ = 1)
LOS H_{25}-H_{25}	horn (25)	horn (25)	1 - 20 (Δ = 1)
LOS H_{15}-O	horn (15)	omni (2)	1 - 10 (Δ = 0.5)
NLOS O-O	omni (2)	omni (2)	2 - 8 (Δ = 1)
NLOS O-H_{15}	omni (2)	horn (15)	2 - 8 (Δ = 1)

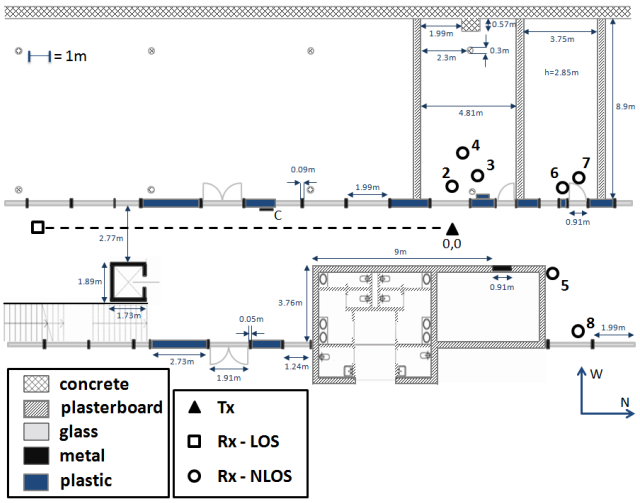

Fig. 1. Measurement environment for the path loss model assumed in the simulations [10].

A. Path Loss Model

The path loss model represents the core of the simulator. We implemented the generalized model proposed in [10], which was obtained through a least-square regression fit of the relationship (1) into the experimental path loss evaluated at all measurement locations at different frequencies, for all measurement configurations listed in Table I, where O, H_{15} and H_{25} respectively refer to omnidirectional antennas, directional horn antennas with a beamwidth of 30 degrees and a gain of 15 dBi, and directional horn antennas with a beamwidth of 9 degrees and a gain of 25 dBi.

The measurement campaign was made in a typical office/lab environment in a modern building at the University of L'Aquila, Italy. The UWB signal used to probe the channel had a bandwidth of 1.2 GHz and was tuned over eight different carrier frequencies spanning the two bands from 54 to 59 GHz and from 61 to 66 GHz.

The measurement scenario is shown in Fig. 1, where all involved materials are specified. As above mentioned, measurements have been done with three different types of antennas, i.e. omnidirectional and directional horn antennas with gain of 15 dBi and 25 dBi, in both LoS and non-LoS (NLoS), as shown in Table I.

For further details about the measurement campaign, we refer the interested reader to [10].

TABLE II
PATH LOSS REGRESSION VALUES

PARAM.	LOS O-O	LOS H_{15}-H_{15}	LOS H_{25}-H_{25}	LOS H_{15}-O	NLOS O-O	NLOS O-H_{15}
n	1.33	1.45	1.7	2.1	1.2	2.4
m	17.4	8.34	9.4	24.5	7	24.7
c	10.68	-3.18	-6.13	4.27	24.2	4.88

TABLE III
STANDARD DEVIATIONS OF SHADOWING

$f_c^{(j)}$ (GHz)	LOS O-O	LOS H_{15}-H_{15}	LOS H_{25}-H_{25}	LOS H_{15}-O	NLOS O-O	NLOS O-H_{15}
54.78	1.39	4.76	1.69	1.08	4.75	2.91
55.98	1.96	1.90	1.30	3.26	3.79	4.15
57.18	3.18	2.03	1.28	3.21	2.97	5.07
58.38	3.39	2.37	3.07	1.81	3.02	6.27
61.78	3.95	1.50	1.25	1.89	2.34	10.74
62.98	2.42	1.44	1.16	2.41	3.34	8.92
64.18	8.99	2.79	7.05	3.60	3.11	9.22
65.38	2.99	2.25	1.39	2.04	3.49	3.70

According to the model in [10], the expression for path loss is derived as an extension of the well known expression of *free space path loss*, and includes both the distance and frequency dependence modeled by power laws [12]–[14]. Hence, the average path loss is given by

$$\begin{aligned} \overline{PL}(f,d)\ [\text{dB}] &= PL(f_0,d_0)\ [\text{dB}] + 10\cdot n\cdot \log_{10}\left(\frac{d}{d_0}\right) \\ &+ 10\cdot m\cdot \log_{10}\left(\frac{f}{f_0}\right) \end{aligned} \quad (1)$$

where $PL(f_0,d_0)$ is the path loss at the reference frequency f_0 and at the reference distance d_0, f is the frequency, d is the transmitter–receiver distance, n is the exponent of the distance power law and m is the exponent of the frequency power law. The distance and the frequency dependence have, generally, different exponents, i.e. $n \neq m$.

The regression fits against all sets of experimental data, returned a set of path loss models whose parameter values are listed in Table II, where c is a constant given by the regression fits and O, H_{15} and H_{25} respectively refer to omnidirectional antennas and directional horn antennas as defined in Table I.

B. The Shadowing Model

Statistical deviations from the deterministic values given by (1) are due to the shadowing, commonly modeled by a lognormal distribution [15], [16]. The shadowing accounts for the small fluctuations in the signal strength related to changes in the surrounding environment due to movements of the receiver. The total attenuation due to the path loss and shadowing is commonly modeled by:

$$PL(d)[dB] = \overline{PL}(d)[dB] + \mathrm{X}_\sigma, \quad (2)$$

where

$$\overline{PL}(d)\ [\text{dB}] = PL(d_0)\ [\text{dB}] + 10 \cdot n \cdot \log_{10}\left(\frac{d}{d_0}\right), \quad (3)$$

where $PL(d_0)$ is the path loss at the reference distance d_0, and the term X_σ, which accounts for the shadowing, is a zero-mean Gaussian variable having a standard deviation σ. Standard deviations for the shadowing term as calculated from the experimental data in [10] for each measurement carrier frequency and setup configuration are listed in Table III.

III. RSSI Localization Algorithms

RSS-based localization systems commonly use two general methods to perform localization, namely *trilateration* and *fingerprinting*. Both require a pre-determined look-up table or model, obtained during an offline phase. In this paper, we consider trilateration, which is a geometrical technique that can locate an object based on its Euclidean distance from three or more objects [17]. This method can be used if the relationship between the RSS and the distance is known, like, e.g., the knowledge of the path loss relationship in (1). Unfortunately, the shadowing introduces uncertainty in the received RSSIs.

We solve this issue, by adopting the following strategy. Each terminal receives the beacons from the APs and obtains the RSSI measurements related to the K APs in its visibility. The i-th terminal stores the RSSI values $w_{i,k}$ measured from the k-th AP. We assume that each terminal is able to collect and store multiple samples $w_{i,k}^{(n)}$, for $n = 1, \ldots, N$ of the measured RSSI from multiple beacons received from the same AP. The terminal creates a $K \times N$ matrix $\overrightarrow{\mathbf{D}}_i$, where the N elements in the k-th row $d_{i,k}^{(n)}$, are the N sample estimated distances from the k-th AP calculated by inverting (1) with $w_{i,k}^{(n)}$ as input values, for $n = 1, \ldots, N$. The estimated distances are affected by a random error due to the uncertainty of the measured RSSI, because of the shadowing phenomenon. Hence, each terminal calculates the mean value $\overline{d_{i,k}}$ and the standard deviation $\sigma_{d_{i,k}}$ of the N samples of estimated distances, as:

$$\overline{d_{i,k}} = \frac{1}{N}\sum_{n=1}^{N} d_{i,k}^{(n)} \quad (4)$$

and

$$\sigma_{d_{i,k}} = \sqrt{\frac{1}{N}\sum_{n=1}^{N}\left(d_{i,k}^{(n)} - \overline{d_{i,k}}\right)^2}. \quad (5)$$

The estimation of the position of the i-th terminal is done by taking the intersections of circles centered in the k-th and the j-th AP for all possible pairs (k, j) and radius $d_{i,k}$ and $d_{i,j}$. If the estimation of distances were perfect, the K circles would intersect in one point where all intersections would coincide, which is the true position of the terminal i.

Due to the uncertainty of measured RSSI values, this fortunate circumstance unlikely happens, but three situations may occur in practice:

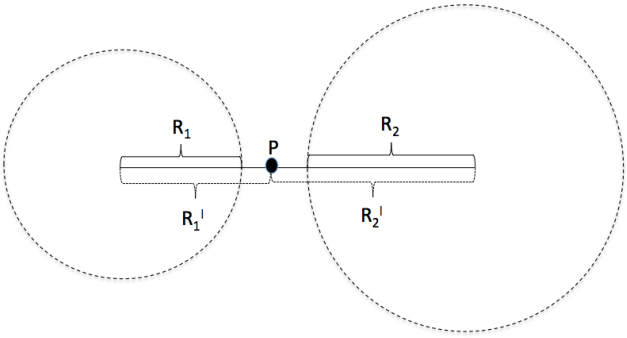

Fig. 2. "Artificial" intersection point in the case that circles do not have any intersection point (**Case 3**).

1) the circles intersect in two points falling within the test area and these points could also be coincident if circles are tangent;
2) the circles have one intersection falling within the test area and one falling outside the test area;
3) the circles do not have any intersection.

Our trilateration algorithm manages the three possible situations according to the following rules:

- **Case 1:** the two intersection points represent two valid points;
- **Case 2:** only the intersection point internal to the test area is considered and the other discarded;
- **Case 3:** an "artificial" intersection point is selected along the line connecting the two circles centres, at a distance based on the weighting of the received power from the two APs.

The **Case 3** is depicted in the diagram of Fig. 2. Given two circles **1** and **2** of rays R_1 and R_2, respectively, with centers located at a distance $R_{12} = R_1' + R_2'$, the position of the "artificial" point P is obtained by

$$R_1' = R_1 \times \frac{R_1' + R_2'}{R_1 + R_2} \quad (6)$$

$$R_2' = R_2 \times \frac{R_1' + R_2'}{R_1 + R_2} \quad (7)$$

where R_1' and R_2' are the distances of P from the centers of circles **1** and **2**, respectively.

The set of obtained intersection points $l^{(i)}$, for $l^{(i)} = 1, \ldots, L^{(i)}$ for the i-th terminal is stored in a vector, I_i; the elements of I_i, i.e. all intersection points, differ from the exact true position of the terminal by a random error $\epsilon_l^{(i)}$, which has a standard deviation given by the quadratic sum of the standard deviations associated to the estimates of distances from the K APs, i.e.

$$\sigma_{\epsilon_l^{(i)}} = \sqrt{\sum_{k=1}^{K}\sigma_{d_{i,k}}^2}. \quad (8)$$

The vector I_i of the intersection points is sorted according to the reciprocal distance values associated to the elements.

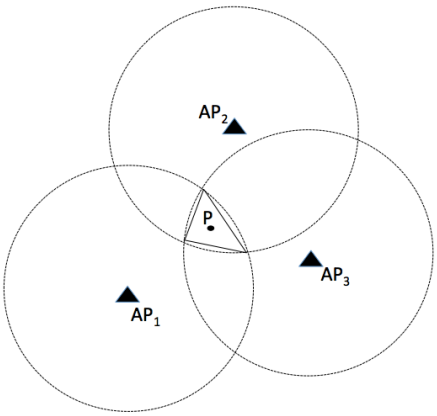

Fig. 3. Selection of the set of h relevant intersection points out of the total $L^{(i)}$ points.

The h closest points out of $L^{(i)}$ are retained and the others discarded. This selection mechanism can be easily explained with the help of the simple diagram shown in Fig. 3. Due to the statistical nature of the shadowing, the three circles depicted in Fig. 3 intersect in $L^{(i)} = 6$ points; $h = 3$ points out of them are closer and can be connected to form a polygon whose vertices are the 3 points. The target point **P** to be localized is likely in the *Center of Mass* of this polygon.

We test two algorithms that differ for the way the center of mass of the h selected points is calculated, i.e.:

- **Algorithm 1 - Center of Mass:** the center of mass is calculated as the midpoint of the h points, referred to as *simple average* in the following;
- **Algorithm 2 - Weighted Center of Mass:** the center of mass is obtained by averaging them by assigning appropriate weights according to their σ_{ϵ_l}, i.e. the points with lower σ_{ϵ_l} have a higher weight, referred to as *weighted average* in the following.

IV. Simulation Setup

We implemented a simulator for the RSSI performance evaluation in Matlab®. We can set the desired test area and the position of the anchors, i.e. the AP. Our performance evaluation assumes an area of 16×8.9 meters. The APs positions are optimized such that maximum coverage is assured, still fulfilling the requirements of the standard concerning the maximum allowed number of APs in a given area.

The number of APs participating in the simulations is varied in order to quantify the improvement provided by an increased number of them. To limit the interference each AP transmits over a specific carrier frequency as specified by the IEEE 802.11ad standard.

The simulator generates a set of random locations P_i for $i = 1, 2, \ldots, 1000$ in the area, which represent the test positions of terminals where the RSSI localization is tested.

RSSI values are calculated for every link between the APs and the positions P_i using the path loss model (1) at the carrier

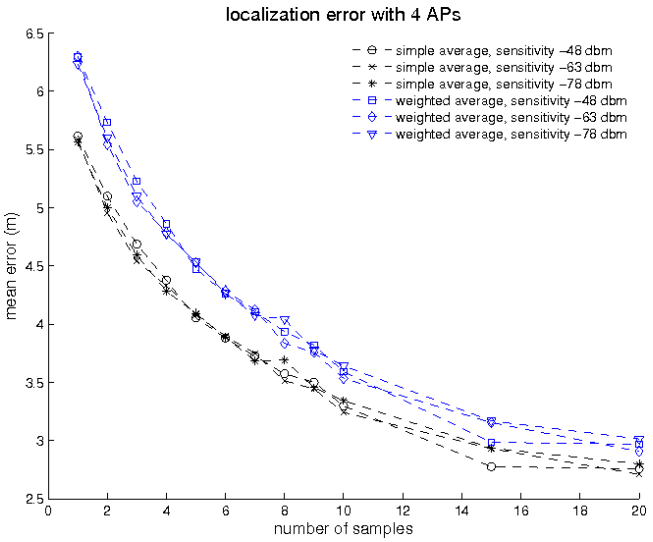

Fig. 4. Mean error of the position estimation made by 4 APs vs. the number of collected samples. As specified in the legend, different curves and markers represent the error for the three different receiver sensitivity levels for the center of mass calculated as either simple mean or weighted average.

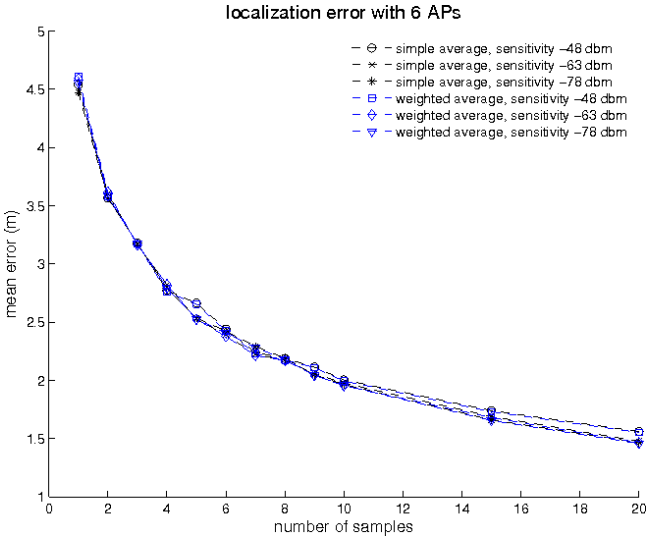

Fig. 5. Mean error of the position estimation made by 6 APs vs. the number of collected samples. As specified in the legend, different curves and markers represent the error for the three different receiver sensitivity levels for the center of mass calculated as either simple mean or weighted average.

frequency assigned to the specific AP and at the distance d_i between the AP and the position P_i.

The deterministic values given by the path loss model are added to a random term that accounts for the uncertainty due to the shadowing. This random term is distributed according to a Gaussian distribution with zero mean and standard deviation dependent on the carrier frequency, as listed in Table III.

We run simulations using a variable number of APs $K = 4, 6, 8$ and three different sensitivity levels of the receiver, set according to the standard for different modulations: either -48 dBm, -63 dBm and -76 dBm. We also varied the number N

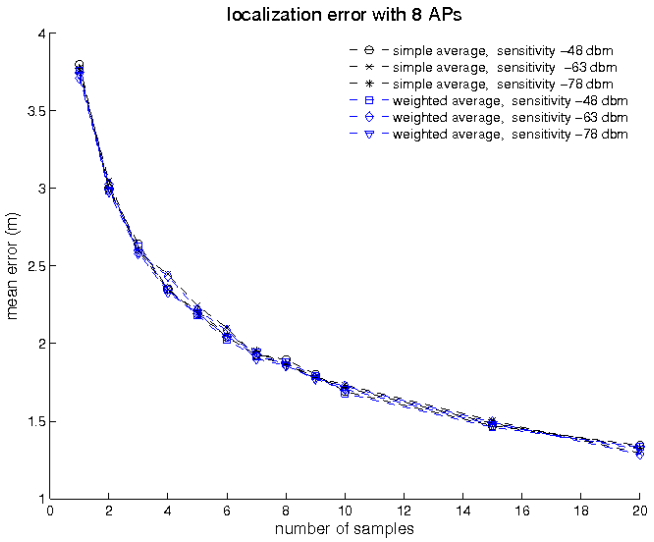

Fig. 6. Mean error of the position estimation made by 8 APs vs. the number of collected samples. As specified in the legend, different curves and markers represent the error for the three different receiver sensitivity levels for the center of mass calculated as either simple mean or weighted average.

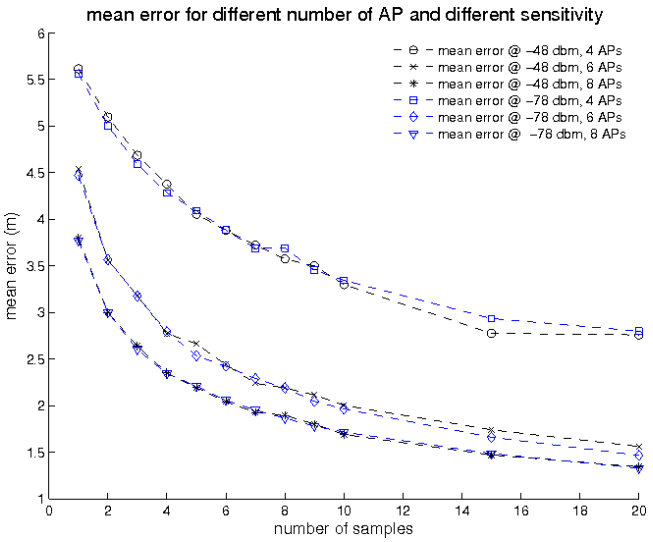

Fig. 7. Comparison of the mean errors vs. the number of collected samples as obtained for the considered scenarios differing by the number of involved APs and the receiver sensitivity. The center of mass is calculated as *simple average*.

of multiple samples collected by the terminal from 1 to 20.

V. Performance Evaluation

Performance is evaluated in terms of mean positioning error in meters and its standard deviation. Fig.s 4, 5 and 6 show the mean error in meter when either 4, 6 and 8 APs are involved in the position estimation, respectively. We observe that the main factor influencing the mean error is the number of collected samples by the terminal. Surprisingly, the use of weighted averages produces a slight degradation of the localization performance with respect to the simple mean in the case of 4 APs, whereas it does not influences performance at all if a number of APs greater than 4 is used. Actually, in the case of an increased number of APs, the simple mean and weighted average curves overlap, showing exactly the same performance. This behavior brings up that the estimation over N multiple samples, with $1 \leq N \leq 20$, is effective for the calculation of the means $\overline{d_{i,k}}$, but the set of samples is not sufficient to provide a reliable estimate of the standard deviation. Increasing the number of APs means increasing the available measurements, thus the imperfect estimation of standard deviation becomes negligible. The localization performance appears independent of the receiver sensitivity for all cases with 4, 6, and 8 involved APs.

Figs. 7 and 8 show a comparison of the mean error and standard deviations vs. the number of collected samples for all cases of 4, 6 and 8 APs for the minimum and maximum receiver sensitivity levels. The center of mass is calculated as *simple average*. We observe that the mean error is not influenced by the sensitivity level, whereas the standard deviation varies up to a 25% for different sensitivity levels. Relevant is the effect of the number of involved APs, with the mean error decreasing from 3 m (case with 4 APs) to 1.3 m (case with 8 APs) in correspondence of 20 collected samples. The gain of using 8 APs instead of 6 APs is small, which does not justify the increase in the processing complexity.

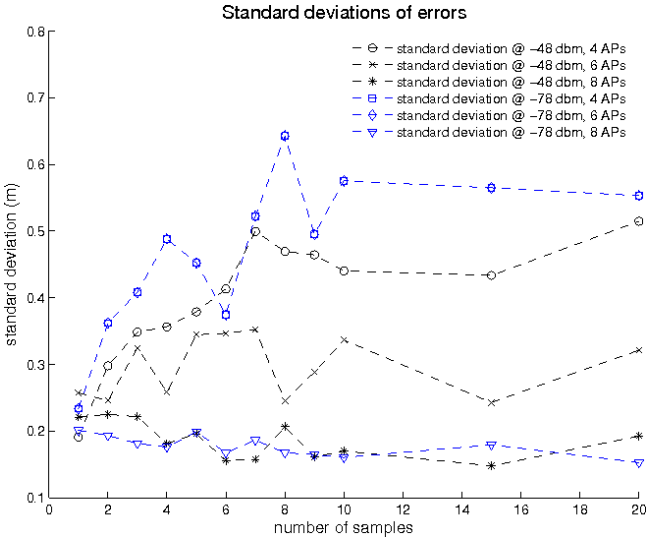

Fig. 8. Comparison of the error standard deviation vs. the number of collected samples as obtained for the considered scenarios differing by the number of involved APs and the receiver sensitivity. The center of mass is calculated as *simple average*.

As shown in Fig. 8, the standard deviation of the positioning error is below 0.5 m for all cases, which is positive.

VI. Conclusion

We analyzed the performances of a localization system based on RSSI for 60 GHz WLANs compliant with the IEEE 802.11ad standard. Performances were evaluated in terms of mean localization error. Two localization algorithms were tested, demonstrating that it is possible to achieve an accuracy

of around 1 m if a sufficient number of measurement samples is acquired. Results also show that the mean localization error significantly improves if the number of APs increases from 4 to 6. The same benefit does not appear if the number of AP is increased to 8. A significant improvement is obtained by increasing the number of samples: simulations show that the mean error could decrease by 60 % if the number of collected samples (beacons) is increased to 15.

ACKNOWLEDGMENT

This work was partially supported by the ERC starting Independent Researcher Grant VISION (Contract n. 240555) and by the MIUR Italian PRIN project GRETA under Grant 2010WHY5PR.

REFERENCES

[1] R. Daniels, J. Murdock, T. Rappaport, and R. Heath, "60 GHz Wireless: Up Close and Personal," *IEEE Microw. Mag.*, pp. 1527–3342, Dec. 2010.

[2] T. S. Rappaport, E. Ben-Dor, J. N. Murdock, and Y. Qiao, "38 GHz and 60 GHz angle-depedent propagation for cellular & peer-to-peer wireless communications," in *Intern. Conf. on Commun. (ICC 2012)*, June 2012.

[3] D. Dardari, A. Conti, U. Ferner, A. Giorgetti, and M. Z. Win, "Ranging With Ultrawide Bandwidth Signals in Multipath Environments," *Proceedings of the IEEE*, vol. 97, no. 2, pp. 404–426, Feb. 2009.

[4] A. Conti, M. Guerra, D. Dardari, N. Decarli, and M. Z. Win, "Network Experimentation for Cooperative Localization," *IEEE JOURNAL ON SELECTED AREAS IN COMMUNICATIONS*, vol. 30, no. 2, Feb. 2012.

[5] F. Mazzenga and M. Vari, "Indoor Localization Techniques based on Active and Passive Devices," in *Proceedings of Emerging Technologies for Radiofrequency Identification (RFIDAYS)*, 2008.

[6] D. D. Luca, F. Mazzenga, C. Monti, and M. Vari, "Performance Evaluation of Indoor Localization Techniques Based on RF Power Measurements from Active or Passive Devices," *EURASIP Journal on Applied Signal Processing*, pp. 1–11, 2006.

[7] M. Bocquet, N. Obeid, C. Loyez, C. Lethien, F. Boukour, N. Rolland, and M. Heddebaut, "Comparison between 60-GHz UWB frequency modulation and UWB impulse-radio location systems," in *Radar Conference, 2008. EuRAD 2008. European*, Oct. 2008, pp. 41–43.

[8] H. R. Fang, G. P. Cao, E. A. Gharavol, K. Tom, and K. Mouthaan, "60 GHz short range planar RSS localization," in *Proceedings of Asia-Pacific Microwave Conference 2010*, 2010.

[9] D. Bojic, E. Sasaki, N. Cvijetic, T. Wang, J. Kuno, J. Lessmann, S. Schmid, H. Ishii, and S. Nakamura, "Advanced wireless and optical technologies for small-cell mobile backhaul with dynamic software-defined management," *Communications Magazine, IEEE*, vol. 51, no. 9, pp. 86–93, Sep. 2013.

[10] S. Piersanti, L. A. Annoni, and D. Cassioli, "Millimeter waves channel measurements and path loss models," in *IEEE ICC 2012*, Jun. 2012.

[11] "IEEE Standard for Information technology–Telecommunications and information exchange between systems–Local and metropolitan area networks–Specific requirements-Part 11: Wireless LAN Medium Access Control (MAC) and Physical Layer (PHY) Specifications Amendment 3: Enhancements for Very High Throughput in the 60 GHz Band," *IEEE Std 802.11ad-2012 (Amendment to IEEE Std 802.11-2012, as amended by IEEE Std 802.11ae-2012 and IEEE Std 802.11aa-2012)*, Dec. 2012.

[12] J. Keignart, "U.C.A.N. Report on UWB Basic Transmission Loss." Tech. Rep. IST-2001-32710 U.C.A.N., Mar. 2003.

[13] A. Armogida *et al.*, "Path-Loss Modelling in Short-Range UWB Transmissions," in *Intern. Workshop on Ultra Wideband Systems*, Jun. 2003.

[14] A. Molisch, "Ultrawideband propagation channels-theory, measurement, and modeling," *Vehicular Technology, IEEE Transactions on*, vol. 54, no. 5, pp. 1528–1545, Sep. 2005.

[15] D. Cassioli, M. Z. Win, and A. F. Molisch, "The UWB Indoor Channel: from Statistical Model to Simulations," *IEEE J. Select. Areas Commun.*, vol. 20, no. 6, pp. 1247–1257, Aug. 2002.

[16] A. F. Molisch, D. Cassioli, C.-C. Chong, S. Emami, A. Fort, B. Kannan, J. Karedal, J. Kunisch, H. G. Schantz, K. Siwiak, and M. Win, "A Comprehensive Standardized Model for Ultrawideband Propagation Channels," *IEEE Trans. on Ant. and Prop.*, pp. 3151–3166, Nov. 2006.

[17] S. Mazuelas, A. Bahillo, R. Lorenzo, P. Fernandez, F. Lago, E. Garcia, J. Blas, and E. Abril, "Robust Indoor Positioning Provided by Real-Time RSSI Values in Unmodified WLAN Networks," *IEEE Journal of Select. Topics in Signal Processing*, vol. 3, no. 5, pp. 821–831, Oct. 2009.